ARTICLE

Check for updates

Southwestern United States drought of the 21st century presages drier conditions into the future

Eugene R. Wahl [1]✉, Eduardo Zorita[2], Henry F. Diaz[3] & Andrew Hoell [4]

Intense drought has occurred in the United States Southwest this century, causing unprecedented stress to water resources. Here we use paleoclimate and instrumental records to establish that the recent temperature rise is incompatible with random draws from past fluctuations, including the current period of warming. Consistent with and extending previous reconstructions, we find that the ongoing drought is the most intense at the 21-year scale back to 600 CE. Evaluation using standardized regression coefficients shows that recent warming damps the effect of moisture delivery on the Standardized Precipitation-Evaporation Index by approximately one-third. The probability of full recovery of the current moisture deficit is unlikely even by mid-century and about five percent in 10-15 years. Evaluation of future climate simulations indicates increasing regional temperature stress and soil moisture depletion, and coupled with long recovery periods for moisture delivery, very low chance for regional mega-reservoirs to regain full-capacity levels assuming current demand.

[1] Independent researcher, Boulder, CO, USA. [2] Helmholtz Zentrum Hereon, Geesthacht, Germany. [3] University of Hawai'i, Manoa, USA. [4] NOAA Physical Sciences Laboratory, Boulder, CO, USA. ✉email: generwahl@yahoo.com

The start of the 21st century CE has witnessed intense drought conditions in the American Southwest (SW). This region—comprising the states of California, Nevada, Arizona, Utah, New Mexico, and Colorado—has a human population of over 60 million, including indigenous peoples and their historical tribal lands (as of 2019)[1]. Economically, the region is responsible for $4.2 trillion annually in the gross regional product (as of 2018)[2], the fourth largest in the world if the region were a separate country[3]; it also includes the largest port complex in North America (Los Angeles-Long Beach, California)[4] and globally important agriculture, information technology, arts, entertainment, media, aerospace, biotechnology, medicine, and associated research industries. It is also home to unique ecosystems and endemic species in its celebrated geological and biogeographic landscapes. The ongoing bidecadal (two or closely approximating two decades in duration) drought has led to historically unprecedented stress on critical water resources in this semi-arid to arid region. In the spring of 2022, North America's two largest reservoirs—Powell in Arizona and Utah and Mead in Nevada and Arizona—were at their lowest levels since initial filling, leading to cessation or reduction of water and electric power deliveries with far-reaching impacts on urban, agricultural, and tribal areas and economies, along with ecosystem and landscape aridification and increased incidence of extreme fires in the region[5–8]. Long-term evaluations of western and southwestern drought conditions in the United States have been developed using paleoclimate and instrumental records in conjunction with simulated future conditions[9–15]. In addition, different aspects of centuries long precipitation variability in the West and California, in particular, have been evaluated, focusing on the moisture delivery side of drought conditions[16,17]. These findings indicate that, since the turn of the 21st century, drought conditions have been prevalent over much of the SW and that, in comparison with several drought reconstructions, average conditions during this period are the most severe in the available paleoclimate record for a drought of this length.

Here, we complement and expand the perspective of prior studies. First, we evaluate the ongoing 21-year drought starting from the perspective of fundamental climatological drivers—precipitation (moisture supply) and temperature (an aspect of moisture demand)—using both instrumental[18] and paleoclimate records[16,17,19] for the Southwest extending into the 16th century, notably including the later 1500's extreme drought in the region (Methods). The ground-up approach of evaluating these drivers separately allows identification of their individual roles in the ongoing drought, along with a formal statistical examination of how likely their current trends are in comparison to these variables' long-term trajectories. It similarly allows quantitative probabilistic evaluation of the likelihood of recovery from the current drought in terms of moisture delivery itself over time frames of the next decade to mid-century. Second, we use these two fundamental drivers in calibration with the Standardized Precipitation Evaporation Index (SPEI)[20] to formulate a new reconstruction of climatological drought in terms of the SPEI that also extends to the later 1500's (Methods). This record complements land surface-oriented metrics that have been used for examination of SW drought[9–11,13–15] by facilitating its evaluation in terms of a measure that has been designed explicitly for global use, including in regions where soil moisture information is sparse or non-existent. We also utilize a spatial drought paleoreconstruction product recently developed by NOAA's National Centers for Environmental Information (NCEI), the Living Blended Drought Atlas[9,21], in order to cross-evaluate this soil moisture-oriented metric (Palmer Modified Drought Index, PMDI) with the purely meteorological SPEI reconstruction. We note that both measures clearly capture the key bidecadal droughts of the past half-millennium, and corroborate recently published analyses[14,15]. They additionally allow independent estimation of the recent enhanced influence of temperature on SW drought conditions (Methods). This empirical evaluation is separate from, but logically parallel to, climate model-based estimates of impact attribution and is consistent with them.

Third, we utilize the PMDI data to search for droughts comparable in intensity and duration to current drought conditions as far back as 600 CE (Methods), extending to that year the recent finding that the current drought is deeper than any reconstructed to occur since 800 CE[15] (evaluated using a 22-year length of period). Fourth, we evaluate upstream atmospheric circulation conditions in the Northeast Pacific for the later 1500's extreme drought[22] in comparison with the current drought[23], which indicates even stronger winter ridging could occur in the future than that associated with the current situation (Methods). Finally, we examine a large suite of climate model simulations (CMIP6-SSP585 scenario[24], along with the similarly strongly forced RCP8.5 scenario and the less strongly forced RCP4.5 scenario used in CMIP5[25]) to evaluate potential future trajectories of temperature, precipitation, and overall levels of aridity[9,11–15] in the SW (Methods). We note that climate simulations to date have provided an uncertain picture of future precipitation trends in the SW, as this region is straddled by the projected tendency towards greater precipitation at high latitudes and drying of subtropical regions[15,26]. By contrast, temperatures are robustly projected to increase in the 21st century[27]. Thus, it is critical to ascertain the specific impact of temperature on drought conditions to reduce the uncertainty in drought projections. In conjunction with the recovery period analysis for precipitation, the simulation output facilitates evaluation of the potential for full recovery from the current unprecedented losses to regional water resources (i.e., with the impact of temperature increases included). Taken together, these results indicate very low likelihood of full recovery within the region and its water storage and distribution systems in the foreseeable future, especially if stronger than current ridging in the Northeast Pacific occurs as it did during the later 1500s drought extreme.

Results

SW temperature and precipitation—16th–21st centuries. The historical reconstruction (RECON) and instrumental (INST) data for annual temperature and water-year (October$_{t-1}$–September$_t$) precipitation (Fig. 1) are dominated by two features: (a) the rise in temperature associated with anthropogenic forcing[27] that becomes evident starting c. 1980 (Fig. 1b); and (b) the low precipitation extremes of the "early" (1571-1590, from the start of the precipitation RECON to a shift to less extreme conditions in 1591) and "current" (2001–2021) approximately bidecadal drought periods (Fig. 1a)[14,15]. The precipitation time series is effectively a white-noise process, with no significant autocorrelation values beyond lag 0 (Supplementary Fig. 1a), indicating that the current dryness, while very strong, is consistent with a random realization of its long-term process. Eight years with values consistently above or below the long-term mean is the longest such span in the precipitation record, the extended wet period in the 1740s (Fig. 1a). [The running 31-year lag 1 correlations for precipitation (Supplementary Fig. 1c) show decadal and multi-decadal variability, as expected from a random process of this kind and which are generally within estimated 95% confidence boundaries.] In contrast, the temperature time series has a strongly significant positive autocorrelation structure (Supplementary Fig. 1b), conforming with persistent runs above or below the long-term mean (Fig. 1b). The most extreme cold period, in the early 1800s, is associated with a cluster of important volcanic
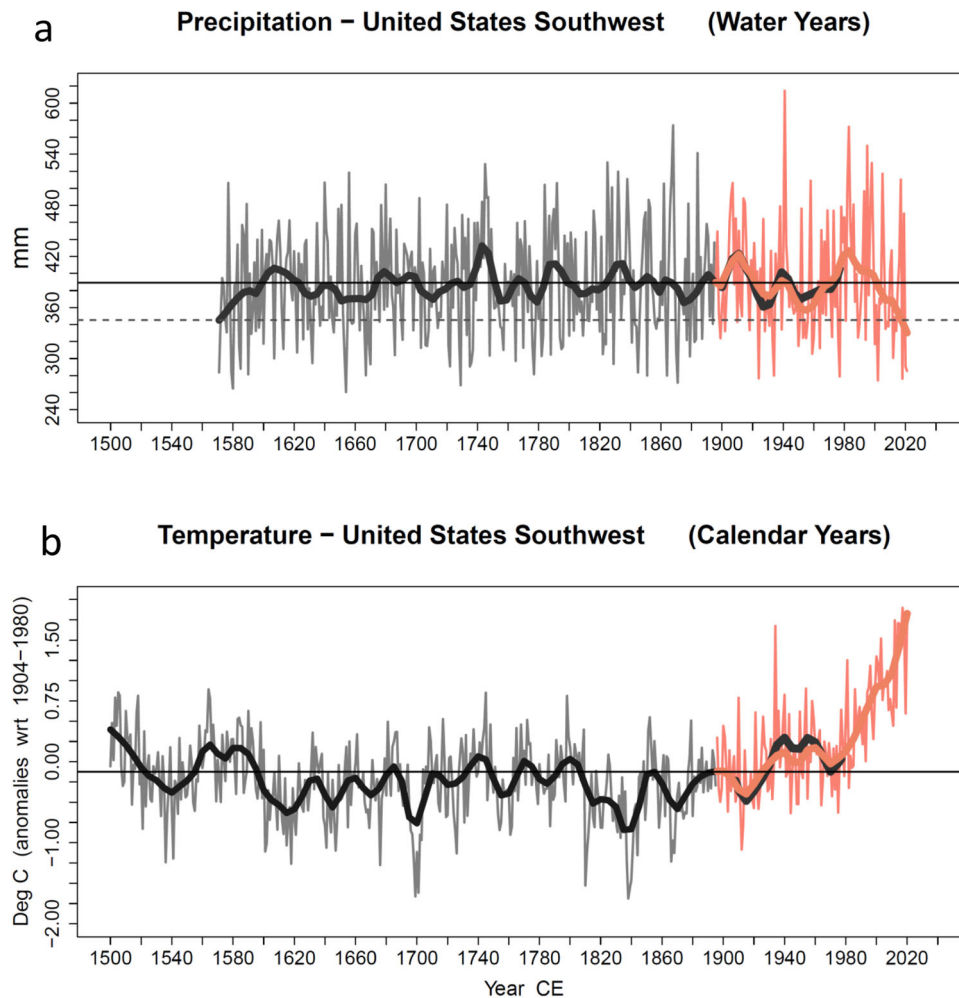
Fig. 1 Southwest historical water year precipitation and calendar year annual mean temperature. Water year (Oct_{t-1} to $Sept_t$) precipitation (**a**), 1571-2021, and calendar year temperature (**b**), 1500-2020, in the SW. Gray and dark gray indicate paleoreconstructions (RECON, through 1895), salmon indicates instrumental (INST, 1896-on) data; heavy lines indicate ~21-year lowess smoothing filters. Solid horizontal lines indicate means of full RECON + INST time series; dashed horizontal line (top) indicates smooth value for 1571. Correlations between RECON and INST smooths during period of overlap (to 1977 precipitation, to 1980 temperature) are 0.88 and 0.92, respectively.

events[28] and the ongoing current warming trend is clearly associated with anthropogenic greenhouse emissions[27], highlighting the sensitivity of regional temperature to large-scale atmospheric forcings. It is notable that the early drought period was not only strongly dry, but also was part of a multi-decadal warm period that was not surpassed until the mid-20th century (Fig. 1b).

The rank results (Fig. 2) extend and further inform what is indicated visually by the precipitation and temperature time series (Fig. 1), that while precipitation currently exhibits 500-year (or longer) low bidecadal-scale levels, temperatures have been exceptional during the ongoing drought. Of the ten joint ranking years (Fig. 2c) with the highest values (representing warm/dry conditions), five have occurred since 2000, and the only other bidecadal or shorter period with more than one of these years is the early drought, with two. The 20-year mean values of the rankings (Table 1) organized by joint ranking from highest (warm/dry) to lowest (cool/wet), similarly isolate how impactful temperature has been in the recent period. While precipitation since 2001 is tied for the third driest average ranking, the temperature rankings show a strong and discrete jump to very high values starting in the 1990s, well beyond the average ranking of any earlier bidecadal period. The increments (deltas) in the joint rankings since 1991 are also unique over the period examined, again reflecting the dominance of increasing temperatures.

A probabilistic perspective (Fig. 3) additionally reinforces these outcomes. Figure 3a indicates the shift in precipitation toward lower values for both the current and early droughts in terms of their estimated probability density functions (PDFs, both considered at 20-year length in this evaluation) compared to the intervening period. Figure 3b shows where the means of these two droughts lie relative to the distribution of 20-year means estimated from Monte Carlo (MC) random resampling with replacement. The means of the current and early droughts lie between −1 and −2 standard deviations (SDs), at the ~9% and ~8% percentile levels, respectively. In contrast, Fig. 3c shows a very strong estimated PDF shift to higher temperatures over the past 40 years (following Fig. 1b), and the mean of this period is ~11 SDs above the mean of the MC estimated distribution of 40-year averages (Fig. 3d). This spectacular distance from the estimated distribution indicates that the current multi-decadal temperature rise has $p = 0$ estimated probability of representing a random realization of the half-millennium temperature process expressed in the SW.

The ensemble climate model (MODEL) characteristics of the temperature and precipitation time series over 1850–2099 (Fig. 4a) are similar to those of the combined RECON + INST data, showing the anthropogenically driven trend in temperature that
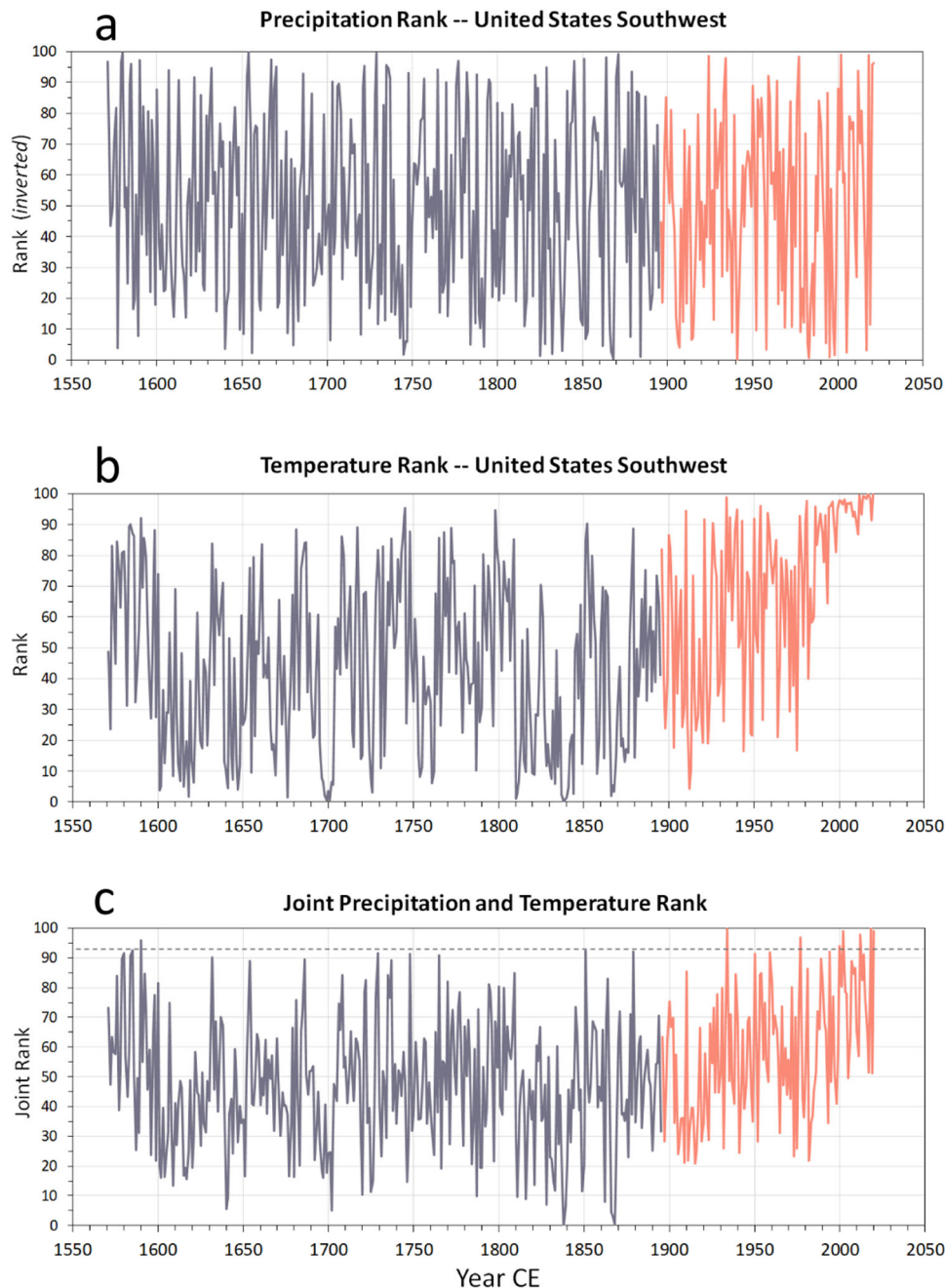
Fig. 2 Southwest historical water year precipitation and calendar year annual mean temperature rank values. Rank values (normalized between 0 and 100) for the SW precipitation (**a**) and temperature (**b**) time series shown in Fig. 1, and joint rankings (**c**); time periods are 1571–2021 for precipitation and 1571–2020 for temperature and joint ranks. Precipitation ranks are inverted so lowest rank represents highest value/highest rank represents lowest value. Color scheme follows Fig. 1. Dashed line in **c** indicates ten years with highest (warm/dry) joint rankings.

begins to separate from its temporal background c. 1980, and the white noise-like character of precipitation which continues throughout the MODEL period with a very slight rise later in this century. The ranking values (Fig. 4c, d) follow the character of the individual temperature and precipitation time series, with a strong upward trend for temperature after c. 1980, effectively random variability for precipitation with the slight rise noted, and increasing joint rankings following the trend in temperature. MODEL soil moisture outcomes are shown in panel 4b (see also below). From a mechanistic perspective, the effect of potential evapotranspiration on soil moisture depends on radiation, vapor pressure deficit, and wind. Vapor pressure deficit itself is dependent on temperature, such that at a given relative humidity

vapor pressure deficit increases with increasing temperature, thereby raising potential evapotranspiration in the absence of changes in wind or radiation[29]. This effect can be seen in Fig. 4a, b for the MODEL simulations, where with little change in precipitation, temperature-driven increases in potential evapotranspiration desiccate the land surface and decrease soil moisture.

SPEI and PMDI—16th–21st centuries. The SPEI provides a quantitative way to evaluate the combined influence of precipitation and temperature more systematically, further extending the individual time series and joint ranking analyses in terms of the moisture balance relationship between delivery (precipitation) and demand (temperature)[20]. SPEI is independent of soil moisture

Table 1 Running bidecadal period rankings for SW historical precipitation and temperature.

		Mean 20-Year Ranks		
Joint	Joint Δ	Start Year	Annual Temp	WY Precip
77	7	*2001*	96	57
70	8	*1991*	92	47
63	1	1571	66	58
62	4	1951	68	55
58	1	1931	64	52
57	0	1791	62	52
57	5	1971	69	44
51	2	1651	41	61
49	0	1731	60	40
49	0	1891	54	45
49	0	1711	46	52
49	0	1751	41	57
49	0	1771	48	50
48	2	1871	42	55
47	1	1671	50	44
46	0	1851	44	48
45	1	1631	39	53
45	0	*1591*	*43*	*47*
45	5	1911	44	46
40	2	1691	31	50
38	2	1811	27	50
36	4	1611	25	48
32	–	1831	22	43

Mean 20-year rankings of RECON + INST temperature, precipitation, and their joint rankings (Fig. 2) along with the increment of the joint rankings between periods. Periods are listed from highest (warm/dry) to lowest (cool/wet) joint ranking. Italics indicate late 1500s drought and period since 1991.
[Note that the rankings shown are averages of the twenty annual values for the period indicated and thus do not extend over the normalized annual range of 0–100].

retention and release[20], intentionally differing in that way from metrics such as the Palmer Drought Severity Index (PDSI)[30] or the PMDI[9,21]. The monthly time-step data we use to construct water year averages (Methods) has an inherently shorter time-lag structure than the Palmer indices, making it better suited to capture seasonal to annual differences in climatological moisture balance without memory effects that are related to soil characteristics per se[20]. The new RECON of SPEI for the SW going back to 1571 (Fig. 5a, Methods), provides an independent complement to the PDSI, PMDI, and other soil moisture reconstructions that have been used for paleo-drought analysis in the region[9–11,13–15,21]. The PMDI parallel to the SPEI RECON (Fig. 5b) is based on the Living Blended Drought Atlas[9,21].

The approximately 21-year smooth curves in Fig. 5 indicate that the SPEI and PMDI results differ in some respects vis-à-vis the amplitude of wet periods of this length, but cohere strongly regarding the three most arid such features of the past 450 years—the early and current droughts along with the previously most intense INST-period drought of the 1950s. Both RECON + INST records indicate that the current drought is the most intense at this scale over their entire length going back to 1571. The PMDI RECON data, per se, extend further back in time and indicate the current drought is the most intense at the approximately 21-year scale in the SW since at least 600 CE (Fig. 6) (Methods), consistent with the recent conclusion that the current drought is the driest of its kind since at least 800 CE[15], and extending that time into the past by an additional 200 years. We note also the recent result (based on limited, very long tree ring data) that streamflow during the current drought in the smaller sub-domain of the SW represented by the Upper Colorado River Basin is experiencing its most intense dry period since the second century CE[31].

We further exploited these metrics to estimate the change in the relative quantitative contributions of temperature and precipitation to the current drought, by regressing them on temperature and precipitation and calculating the standardized regression coefficients (β weights) of these two predictors (Methods). This analysis provides estimates of 34% (INST SPEI) and 37% (RECON + INST PMDI) reductions in the role of precipitation versus temperature during the current drought, which are broadly consistent with recently reported estimates of a 33–46% increased role for combined anthropogenically driven trends in temperature, precipitation, and relative humidity[14,15,32] including the most recent value of 42%, also through 2021[15]. In conjunction with the probabilistic evaluation that the current rise in temperature cannot be viewed as a random realization of the half-millennium-long temperature process expressed in the SW, our estimates of the reduced role of precipitation relative to temperature represent strictly empirical evaluation of the role of anthropogenically-forced temperatures in the current drought: separate from, but logically parallel to formal climate model-derived attribution.

Calibration of the MODEL soil moisture (Fig. 4b) to the INST SPEI and the PMDI (Methods) provides a self-consistent view of the SW moisture balance from 1571-2099. Possible future trajectories under the CMIP6-SSP585 scenario (Fig. 5) are indicated by box-and-whisker plots and black dashed lines (see ref. [11] for a similar evaluation with the CMIP5 simulations). The MODEL output is highly variable, including the possibility of quite high (wet) SPEI or PMDI values, represented by their 80th percentile levels. However, the MODEL expected value (EV) outcomes indicate strongly negative moisture balances in the SW through the 21st century, and the 20th percentile values are extremely negative and far outside the historically observed range of RECON + INST. When joined with the return-time analysis for precipitation noted below, these potential outcomes suggest that recovery to prior moisture balance conditions from the current drought in the SW, in terms of both temperature and precipitation, is even more unlikely than the low likelihood for recovery estimated in terms of precipitation itself.

Recovery time for precipitation from current deficit. We additionally estimated the time span needed for potential recovery of SW cumulative precipitation from the current deficit to climatological normal conditions[17] (Methods). The shortest estimated potential recovery time in the SW RECON + INST precipitation record is five years, associated with the wettest run of years in the 1740s (Fig. 1a). Overall, only 2.9% of recovery values represent periods of ≤10 years, 6.0% represent periods of ≤15 years, 8.4% represent periods of ≤20 years, and 13.6% represent periods of ≤30 years, which would be essentially to the mid-21st century. The mid-century value represents 1 to 6.4 odds —based entirely on precipitation itself—without considering the changed evapotranspiration demand from projected temperature and CO_2 increases[33,34] and second-order effects such as runoff and soil moisture timing changes due to less precipitation delivered as snow and more as rain, and potential vegetation changes[35–37]. We note that these evaluations into the future assume that regional precipitation continues to act as effectively a white noise time series (Supplementary Fig. 1a), as the MODEL output suggests (Fig. 4a).

Circulation conditions of current and 16th century droughts. Finally, we evaluated the hypothesis that atmospheric circulation conditions associated with the early drought were stronger than those during the current drought since anthropogenically elevated temperatures were not involved earlier[14]. To evaluate this
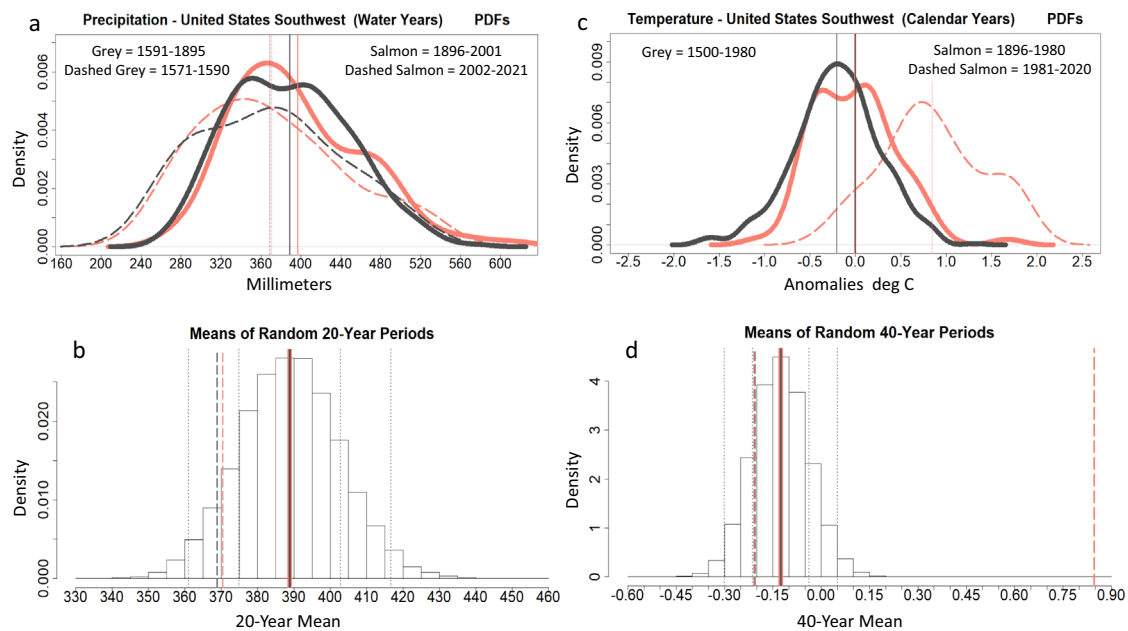
Fig. 3 Probabilistic characteristics of Southwest historical water year precipitation and calendar year annual mean temperature. a solid curves show estimated PDFs for RECON (dark gray) and INST (salmon) precipitation data, removing earliest and most recent 20-year periods (1571–1590 from RECON and 2002–2021 from INST). Solid vertical lines indicate means of the retained time periods (1591–1895 for RECON and 1896-2001 for INST). Dashed curves show estimated PDFs for 1571–1590 and 2002–2021 drought periods and dashed vertical lines their means. **b** Histogram of means of random 20-year samples (with replacement, $n = 10,000$) from full RECON + INST precipitation time series. Solid vertical line indicates overall mean of sample means. Dashed vertical lines indicate means of 1571–1590 and 2002–2021 periods, as above. Dotted vertical lines indicate + -1 and + -2 SDs for overall mean. **c** Solid curves show estimated PDFs for RECON (1500–1980) and INST temperature data (1896–1980, removing the most recent 40-year period). Solid vertical lines at 0 indicate mean over 1896–1980 for INST and over recalibration period (1904–1980) for RECON. Solid vertical line near −0.2 indicates RECON data mean over 1500–1980 period. Dashed curve shows estimated PDF for 1981–2020 and dashed vertical line its mean. **d** Histogram of means of random 40-year samples (with replacement, $n = 1,000,000$) from full RECON + INST temperature time series. Solid vertical line indicates overall mean of sample means. Dashed vertical line near 0.85 indicates mean of 1981–2020 period, as above. Dashed salmon-gray vertical line indicates 1500–1980 mean for RECON + INST data. Histogram y-axis values represent relative densities, not densities normalized to 1.

hypothesis, we use winter (DJF) sea level pressure (SLP) RECONs in the northeastern Pacific for the early drought[22] and corresponding reanalysis data[23] for the current drought (Fig. 7). For this wintertime season, in which much of the SW's precipitation is delivered[38], composite SLP ridging is clearly stronger during the early drought. We note that while the significance of the differences is statistically strong ($p ≤ 0.1$, *using t-test*) in a small portion of the domain, due to the small sample size ($n = 20$) and relatively large variability within the samples, reduction of significance between $p = 0.1$ and $p = 0.2$ occurs only slowly with distance away from the maximum region. This result concerning upstream atmospheric circulation conditions highlights the role that elevated temperatures are playing currently, notwithstanding that precipitation during the current drought is at rare low levels from a half-millennium perspective. The outcome indicates that, separate from ongoing directional increases in regional temperature, composite circulation conditions more extreme than those associated with the present bidecadal drought are clearly possible within the historical and existing climate envelope. Coupling similar more extreme circulation conditions with further forced temperature increases presents the possibility for multi-decadal droughts going forward that significantly exceed the current aridity.

Discussion and conclusions
Our results present a coherent indication that the ongoing bidecadal drought is highly likely the beginning of consistently drier conditions in the SW (see also Williams et al.[15]). Our

analyses indicate that, from a multi-decadal perspective, typical future conditions could well be more like some of the driest periods that have occurred in the historical record and could potentially surpass them[11,15]. The coupling of the empirical recovery time results for precipitation delivery with both the analysis of the to-date shift in the regional temperature distribution and simulated future trajectories for SW temperature strongly suggests that an overall drier moisture regime is already at hand—in effect, ongoing and intensifying aridification. From the dynamical circulation perspective, composite cool-season SLP ridging in the northeastern Pacific associated with low moisture delivery is indicated as notably stronger for the later 1500s drought than the ridging associated with the current drought. A combination of increasing temperatures with a period of such stronger-than-current composite ridging would very likely produce combined precipitation and temperature conditions well into the dry tail of possible future outcomes, with the compounded consequences for society and natural ecosystems that such a period of extreme aridity would present. As an example, the empirical results and simulations strongly suggest that the major SW water reservoirs currently at very low levels are very unlikely to recover to full-pool levels in the foreseeable future, under the assumption that demand continues at current levels. Within that context, our results indicate that it would take unlikely, strong moisture delivery in the next ten to fifteen years —estimated to represent 3% and 6% chances, respectively—to allow recovery to be even somewhat possible in the face of the rising temperature influence. A related conclusion has been determined by the NOAA Drought Task Force, who state,
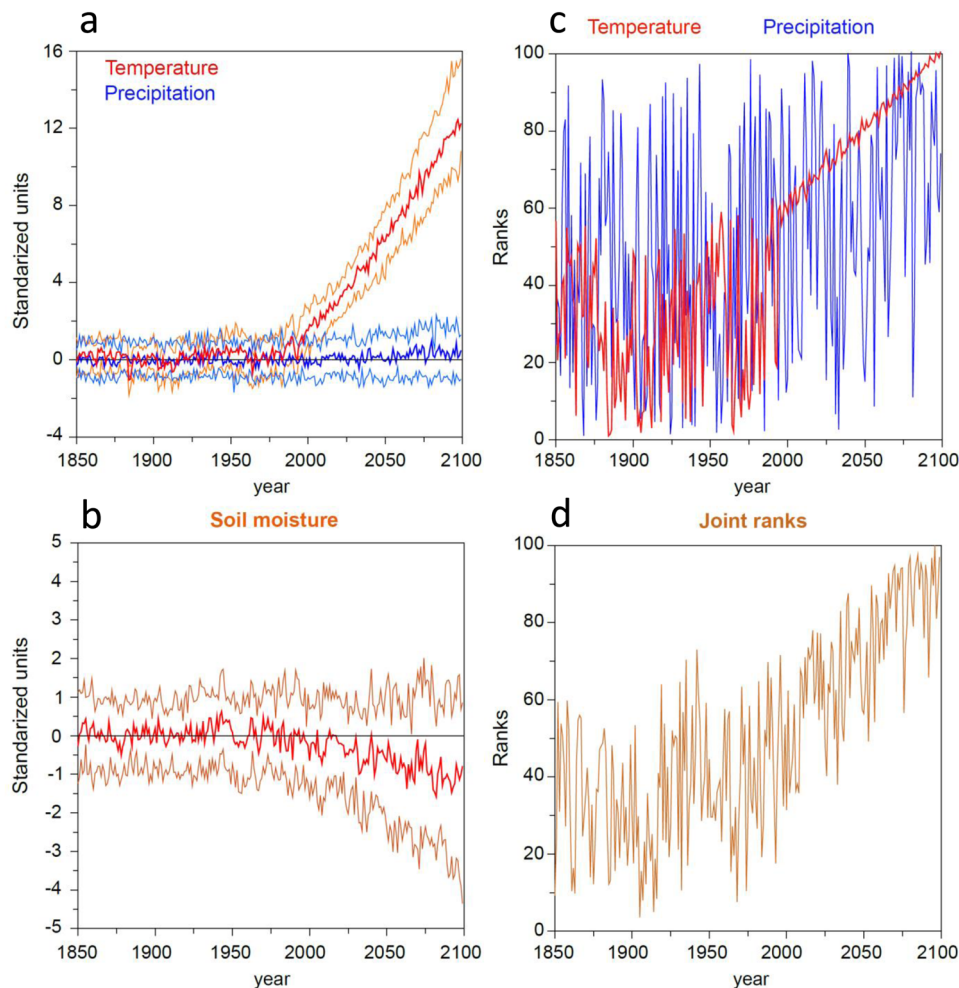
Fig. 4 Model ensemble output for Southwest precipitation, temperature, soil moisture. MODEL (CMIP6, SSP585) ensemble temperature and precipitation (**a**), soil moisture, **b**, and temperature, precipitation, and joint rankings (**c**, **d**). **a**, **b** show 20th and 80th percentile values along with ensemble median. **c**, **d** show median values; 20th and 80th percentile values are highly similar in structure. Rankings are normalized between 0 and 100.

"several seasons (or years) of above-average rain and high elevation snow are needed to refill rivers, soils, and reservoirs across the region"[8,39]. As shown herein, this outcome is highly unlikely to occur in a continuous sequence given the white noise-like nature of regional precipitation (Fig. 1a, Supplementary Fig. 1a, b), which is simulated to continue essentially uninterrupted from the historical regime throughout the 21st century (Fig. 4a).

Our evaluations of potential future outcomes necessarily depend on the trajectories of temperature and precipitation from the MODEL simulations. That precipitation would continue relatively the same as it has historically, with an ongoing white noise-like character, is somewhat difficult to gauge. Regional MODEL precipitation outcomes are known to be highly variable and can embody amplitudes that are substantially different from both INST and RECON values[26], and this is true of the simulations employed here for the SW. However, earth system models of the CMIP6 suite are among the most advanced platforms available for scenario evaluation, and their internally consistent physics represent the best tool available for this purpose. The simulated increases in temperature are a much more clear outcome than the simulated changes in precipitation[26] and are entirely consistent with simple energy balance formulations of the effect of anthropogenic forcing that enhances the retention of outgoing longwave radiation by the atmosphere[40]. Rising temperatures will, by themselves, lead to more precipitation delivery

as rain and less as snow[41,42]. The loss of snowpack and related earlier drying of winter-moist soils in spring[35,43,44] will in turn have major impacts in the SW, given the importance of mountain snow as a critical water reservoir in the region and the non-capture of excess runoff that higher extreme rainfall can possibly entail. Related vegetation drying and high temperature "fire weather" impacts on fire regimes are also indicated and have already been detected[43]. We highlight that our conclusions are affected to only a minor degree by differences between the CMIP6 MODEL outcomes we evaluate and those of its predecessor model intercomparison project, CMIP5, for both the strongly forced RCP 8.5 and less strongly forced RCP 4.5 scenarios of atmospheric composition (Fig. 5). While distinctions between these scenarios can drive significant differences during the 21st century in terms of, e.g., the transient impact of sea level rise on property inundation and values[45], for the SW the conclusion of ongoing and increasing aridity during the rest of the 21st century is little affected—indicating relative robustness of this outcome in relation to these scenario and model platform differences[15].

Data and methods

Temperature and precipitation—instrumental data and reconstructions. INST values for temperature and precipitation were accessed from the Climate at a Glance data portal of
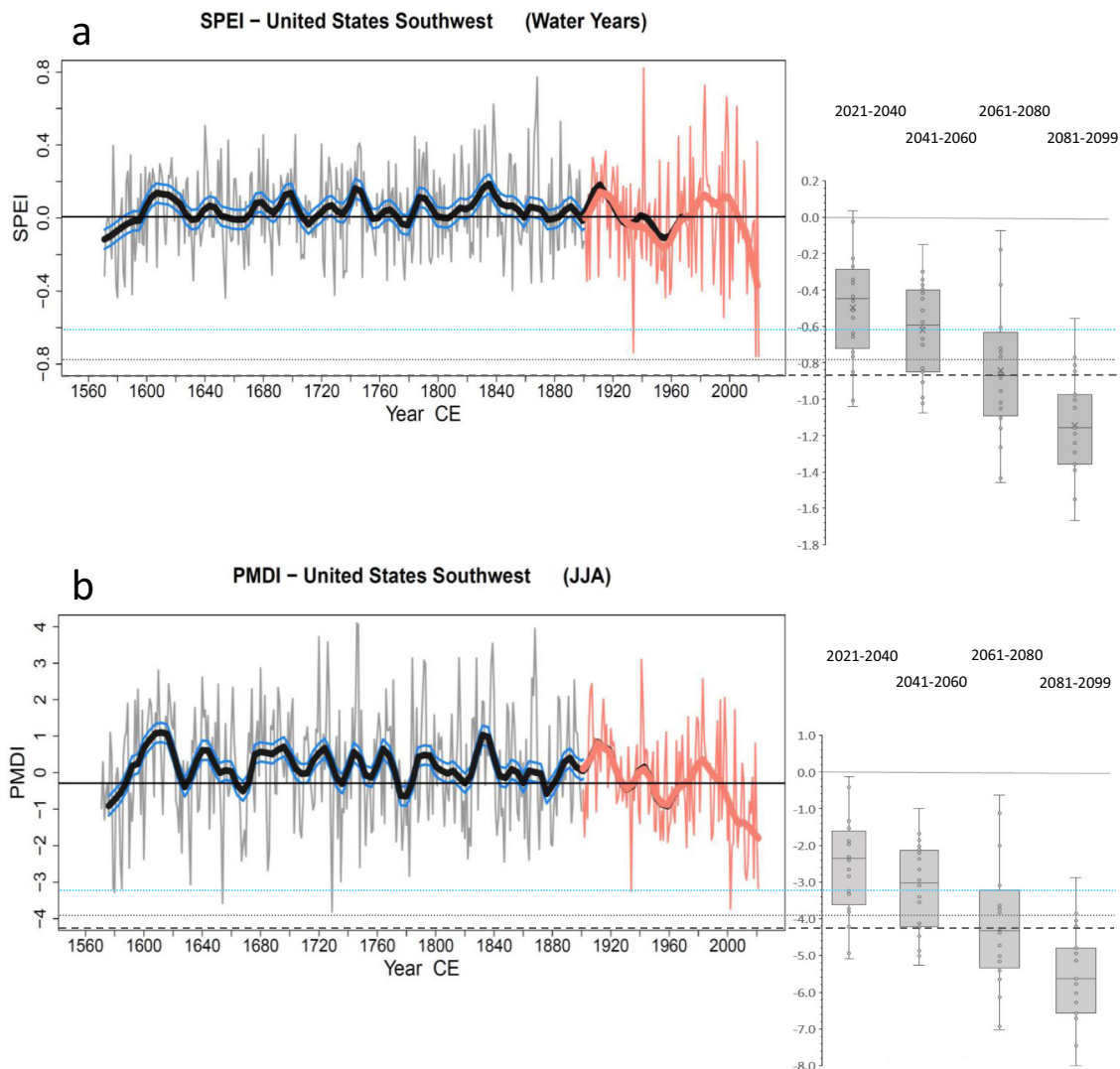
Fig. 5 Standardized Precipitation-Evaporation Index and Palmer Modified Drought Index values for Southwest over 1571-2099. Color scheme for reconstructed (gray) and instrumental (salmon) SPEI (**a**) and PMDI (**b**) values follows that of Figs. 1–3; smooth is ~21-year lowess. Solid black lines indicate mean of INST SPEI and PMDI values (1901–2021) and 0-value during MODEL (CMIP6, SSP585) period (2021–2099); solid blue lines indicate estimated 95% CIs for smooths during RECON period (Methods); box-whisker plots indicate distributions of MODEL median values for four periods during 2021–2099; black dashed line indicates mean of MODEL median values over 2041–2099. Means of MODEL 20th/80th percentile values over 2041–2099 are −2.8/1.1 for SPEI and -13.3/4.7 for PMDI (*values exceed graph scales*). Dotted black (RCP 8.5) and blue (RCP 4.5) lines indicate means of MODEL median values from CMIP5 models over 2041–2095. Correlation between RECON and INST smooths during period of overlap is 0.93 for SPEI; RECON and INST values are the same for period of overlap shown for PMDI (1901–1978) since values for that period are taken from INST. Box-whisker plots show data median (line in box), mean (x in box), first and third quartiles (box bottom and top) and range of data (whiskers).

NOAA's National Centers for Environmental Information (NCEI)[18]. Regional SW values were computed as area weighted averages of NCEI's "West" (California and Nevada) and "Southwest" (Arizona, Utah, New Mexico, and Colorado) regional data. Precipitation data are for water years (WYs, $October_{t-1}$–$September_t$) and temperature data are for calendar years (CY, $January_t$–$December_t$), thereby being fully comparable with the temporal definitions of the temperature and precipitation RECON data.

We employ the RECON temperature data of Wahl and Smerdon[19], which have been used previously for evaluation of last millennium temperature in North America[19,46,47]. The RECON precipitation data are from Wahl et al.[17], and have been used previously both for evaluation of California hydroclimatology[16,17,22,35] and as a partial basis for reconstruction of boreal winter circulation conditions in the northeastern

Pacific and adjacent western North America[22,35]. The temperature RECON data are at a 5°grid scale, and the seven cells that conform most closely with the spatial definition of the SW as mentioned for the INST temperature and precipitation data were extracted (center latitudes 32.5°, 37.5° N; center longitudes −122.5°, −117.5°, −112.5°, −107.5° (W); no data for 32.5°/ −122.5°). The precipitation RECON data are at the 0.5° scale, and thus were able to be conformed closely to the SW spatial definition. The following transformations were applied to ensure compatibility between the temperature and precipitation RECON and INST data: a) the INST and RECON temperature data were set to match as zero-anomalies relative to 1904–1980 (the RECON temperature calibration period), their SDs over this time are essentially identical; the RECON precipitation data were centered and scaled to match the INST precipitation data over 1916–1977 (the RECON precipitation calibration period).
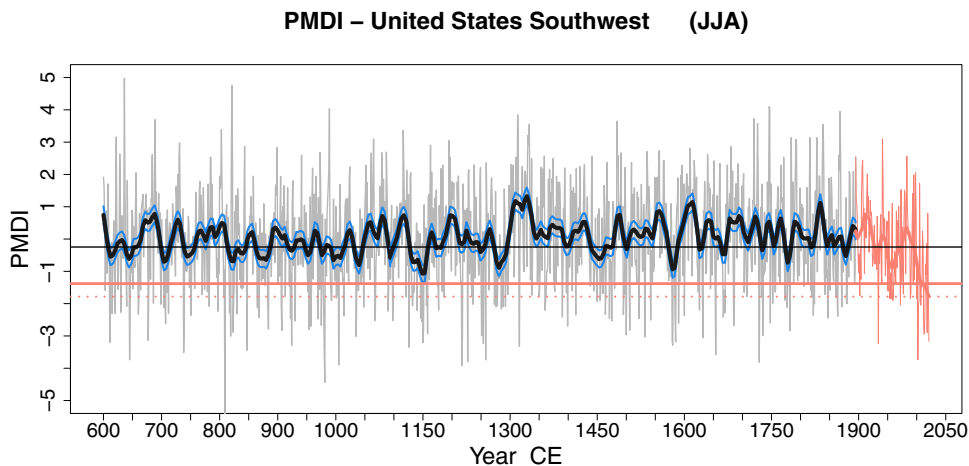
PMDI – United States Southwest   (JJA)

Fig. 6 Palmer Modified Drought Index extended to 600 CE. As Fig. 5b for RECON and INST periods, showing RECON extended to 600 CE (Methods). Solid horizontal salmon line indicates mean of lowess smooth for 2001–2021, dotted horizontal salmon line indicates value of lowess smooth for 2021. Note lower value of estimated 95% CI for 1149 smooth (driest year of mid-12th century drought) is 0.034 PMDI units less dry than lowess mean for 2001–2021.
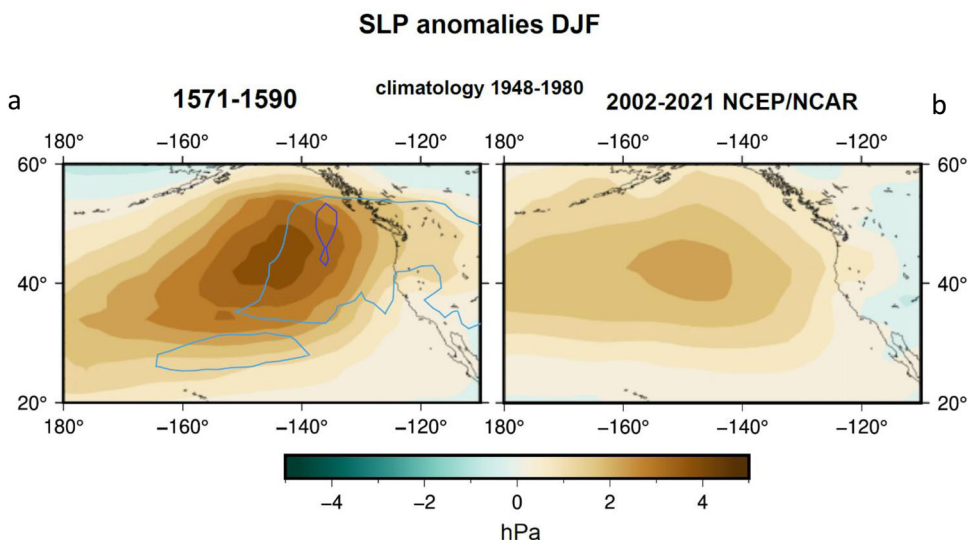

SLP anomalies DJF

Fig. 7 Circulation pressure conditions associated with early (1571-1590) and current (2001-2021) Southwest drought periods. Boreal winter (DJF) SLP composite anomalies for the northeastern Pacific and western coastal North America for **a** early (RECON) and **b** current (INST) drought periods. Climatology period for anomaly calculation is 1948–1980 (the period of overlap between the RECON and INST data) and the mean and standard deviation of RECON data were set to match those of INST during this period to facilitate cross-comparison of the composites. Blue/dark blue contours indicate significance of the differences between the composites at $p \le 0.2/p \le 0.1$ levels, using a 1-sided, inhomogeneous variance t test.

The temperature and precipitation RECONs represent the EV time series from their corresponding ensemble outputs. We focus our evaluation on the EV because it is fully sufficient for the analytical purposes of this paper: to characterize the temperature rise associated with anthropogenic forcing that is evident starting c. 1980 and to identify extreme dry bidecadal periods within the precipitation record that are comparable in depth to the current period. Both features are clearly identified in the EV. Additionally, we note that the RECON bidecadal smooths exhibit high correlation with their INST targets during their comparable periods: 0.92 for temperature and 0.88 for precipitation (Fig. 1). Additional information regarding the temperature and precipitation reconstructions is provided in the Supplementary Methods, Temperature and Precipitation Reconstructions—Additional Information.

Recovery time for precipitation from current deficit. To evaluate potential recovery to mean long-term moisture delivery in the SW from the current drought, we utilized the method of

Wahl et al.[17] to estimate the time for recovery in California from the severe drought of 2012-2015. The whiteness of the precipitation data (Supplementary Fig. 1a) allows us to examine recovery times from a specified initial precipitation deficit without conditioning the examination on the characteristics of the immediately preceding years; i.e., the analysis does not need to depend on examining conditions after a run of particularly dry years, but rather can evaluate recovery time from a specified deficit for all possible starting years since the data lack temporal dependence. Length of recovery is defined to be the number of years it takes for the cumulative regional precipitation to equal or exceed the cumulative climatological average precipitation over the same number of years, when the cumulative total is initialized at the start of the recovery period by the current drought's loss. Recovery periods were evaluated up to 75 years in length; we thus needed to stop the analysis in the mid-1940s going forward from 1571. Again because of the whiteness exhibited by the data, the recovery length analysis can logically be run in reverse,

starting at nearer years and proceeding backward in time, allowing us to fill in the later starting years[17]. As noted by Wahl et al.[17], the recovery length evaluation can be slightly biased if the mean of the RECON data does not match that of the INST data, and thus the mean of the precipitation RECON over its full period (1571-1977) was set equal to the INST period mean for this analysis.

SPEI—instrumental data and reconstruction for SW. SPEI gridded INST data were accessed from the Spanish Consejo Superior de Investigaciones Científicas (CSIC)[20], at 0.5°grid cell scale. The same grid cells used for RECON precipitation were averaged over the WY months. The 2020 value is not available and was estimated to be the same as that of 2018, whose combination of temperature and precipitation values is highly similar to that of 2020. The CSIC index we used represents monthly-scale data, which is the finest time scale available and has no added autocorrelation. We then averaged the monthly-scale information into WY averages for each grid cell.

SW SPEI was reconstructed for the pre-INST period by regressing regional average INST SPEI on INST temperature and precipitation, representing the fundamental climatological drivers of moisture balance—precipitation vis-à-vis supply and temperature vis- à-vis demand. The statistical model is of high quality; with Pearson's r of 0.89 between annual-scale fitted and actual values, SE of 0.145, and very high statistical significance—p-values are 0 (to six significant digits) for t-tests of both predictor variable coefficients and the intercept, along with the F-test for the regression overall. The residuals are well-behaved; their normal probability quantile-quantile relationship is approximately linear supporting the condition that the error terms are normally distributed, they exhibit low first-order autocorrelation (0.107), and the residual vs. predictand relationship for both predictors is effectively homoscedastic. We note that the predictors are empirically nearly independent of each other, with a cross-correlation of -0.11, thus not presenting concerns regarding impacts of predictor collinearity on the estimation of the regression coefficients and corresponding regression outcomes. As a check regarding using this model in the RECON period, we repeated the regression using RECON temperature and precipitation as predictors against INST SPEI. This model mimics that derived using all INST data nearly exactly, with r of 0.97 between the two time series and slightly higher r between fitted and actual values of 0.91—acting indirectly as a separate validation of the temperature and precipitation RECONs. This parallelism also highlights the importance of the role of the *predictands* in the underlying temperature and precipitation reconstructions, in which there is partial overlap of the western North American tree ring chronologies used as predictors (either primarily in the case of temperature, or ultimately in the case of precipitation, whose immediate predictors are streamflow reconstructions—see Supplementary Methods, Temperature and Precipitation Reconstructions—Additional Information). The influence of the predictand temperature and precipitation variables helps drive the empirical near independence of these reconstructions, as in the corresponding INST data.

There is also partial overlap of the predictors used by Williams et al.[15] in their reconstruction with those employed in the temperature and precipitation reconstructions. Their reconstruction is more like the Living Blended Drought Atlas PMDI reconstruction developed by NCEI[21] (see below), and while the PMDI and SPEI reconstructions cohere strongly regarding the three most arid bidecadal features of the past 450 years, they differ in meaningful respects vis-à-vis the amplitude and trend of

bidecadal wet periods. At the annual scale, they differ to the extent that nearly three-eighths of their variance is unshared.

We determined confidence intervals (CIs) for the SPEI reconstruction using the standard formula for the standard error of prediction (SEP) in multiple regression, applied at the 95% two-sided t-distribution critical values; employing extremes of the predictor data where new predictor values occur in the formula to provide a conservative estimation of the CIs throughout the RECON time period. The corresponding CIs for the ~21-year lowess smooths of the reconstructions were derived by dividing the annual time-step CIs by ($\sqrt{21}$) since the smooth values approximately represent 21-year averages.

To estimate the change in the relative quantitative contributions of temperature and precipitation to the current drought, we regressed SPEI on temperature and precipitation and calculated the standardized regression coefficients (β weights) of these two predictors. As noted in the primary text, the INST SPEI data indicate that the influence of precipitation relative to temperature has decreased by 34% for the recent drought compared to the mean of the running 21-year periods since 1900 (21-year spans allow applying each period to its center year). The SPEI RECON has a numerical limitation to extend this analysis into the pre-INST period since it is based on a regression calibration to the temperature and precipitation data. The contribution of the "raw" (unstandardized) regression coefficients to the β weights for each running 21-year period is thus constant over the RECON data, and differences between the estimated β weights are driven solely by the relative variabilities of the reconstructed SPEI and the temperature and precipitation data for each period. These variabilities are strong and lead to an estimated 56% decrease in the influence of precipitation relative to temperature for the recent drought compared to the mean of the running 21-year periods since 1571, which is conceivably an overestimate in light of the white noise-like character of the full RECON + INST precipitation time series (Supplementary Fig. 1a). Performing the same evaluation with the PMDI RECON data provides independent β weights for each bidecadal period and gives an estimate of 37% reduction in the influence of precipitation relative to temperature during the recent drought, compared to the mean of running 21-year periods over the entire 1571-2020 record. See Supplementary Methods, Determination of precipitation and temperature β Weights from the Living Blended Drought Atlas PMDI RECON Data for additional information concerning estimation of the precipitation and temperature β weights from the PMDI RECON data.

Living Blended Drought Atlas—reconstruction and instrumental data. The Living Blended Drought Atlas is a combined RECON + INST product produced by NCEI-Paleoclimatology/World Data Service for Paleoclimatology[21]. It provides 0.5° gridded values of the PMDI, recalibrated by NOAA using updated INST data against the corresponding original RECON[9]. We note that the Living Blended Drought Atlas PMDI record extends in time to 0 CE, however, the tree ring chronology data on which it is based become more-and-more sparse in its early extent. We have set the beginning year for its use in the SW at 600 CE. This date reflects the fact that nearly all the grid cells in the SW domain are represented in the reconstruction to this time (>99%), and then begin to drop out more as time progresses further into the past. A grid cell can drop out of the PMDI reconstruction going back in time for one or both of two reasons: (a) it no longer calibrates or validates successfully; or (b) it shows poor similarity to the reconstruction for the cell done with the most well-represented set of tree-ring predictors during their period of overlap[9]. Setting 600 CE as our earliest year for

Table 2 List of primary (CMIP6) climate models used in this study.

Model	Institution
ACCESS-CM2	Commonwealth Scientific and Industrial Research Organisation,Australia
ACCESS-ESM1-5	Commonwealth Scientific and Industrial Research Organisation,Australia
BCC-CSM2-MR	Beijing Climate Center Climate System Model, China
CAMS-CSM1-0	University Corporation for Atmospheric Research,USA
CAS-ESM2-0	Chinese Academy of Sciences Earth System Model
CESM2-WACCM	University Corporation for Atmospheric Research,USA
CESM2	University Corporation for Atmospheric Research,USA
CIESM	University Corporation for Atmospheric Research,USA
CMCC-CM2-SR5	Fondazione Centro Euro-Mediterraneo sui Cambiamenti Climatici, Italy
CMCC-ESM2	Fondazione Centro Euro-Mediterraneo sui Cambiamenti Climatici, Italy
CNRM-CM6-1-HR	Centre Européen de Recherche et de Formation Avancée en Calcul Scientifique, France
CNRM-CM6-1	Centre Européen de Recherche et de Formation Avancée en Calcul Scientifique, France
CNRM-ESM2-1	Centre Européen de Recherche et de Formation Avancée en Calcul Scientifique, France
CanESM5-CanOE	Canadian Centre for Climate Modelling and Analysis, Canada
CanESM5	Canadian Centre for Climate Modelling and Analysis, Canada
E3SM-1-1	Lawrence Livermore National Laboratory, USA
EC-Earth3-CC	European community Earth-System Model, Europe
EC-Earth3-Veg	European community Earth-System Model, Europe
EC-Earth3	European community Earth-System Model, Europe
FGOALS-f3-L	State Key Laboratory of Numerical Modeling for Atmospheric Sciences and Geophysical Fluid Dynamics, China
FGOALS-g3	State Key Laboratory of Numerical Modeling for Atmospheric Sciences and Geophysical Fluid Dynamics, China
FIO-ESM-2.0	First Institute of Oceanography Earth System Model, China
GFDL-ESM4	Geophysical Fluid Dynamics Laboratory,US
GISS-E2-1-G	NASA Goddard Institute for Space Studies,US
HadGEM3-GC31-LL	Hadley Centre for Climate Prediction and Research, UK
HadGEM3-GC31-MM	Hadley Centre for Climate Prediction and Research, UK
INM-CM4-8	Russian Institute for Numerical Mathematics
INM-CM5-0	Russian Institute for Numerical Mathematics
IPSL-CM6A-LR	Institute Pierre Simon Laplace, France
MCM-UA-1-0	University of Arizona, USA
MIROC-ES2L	University of Tokyo/NIES/JAMSTEC
MIROC6	University of Tokyo/NIES/JAMSTEC
MPI-ESM1-2-HR	Max-Planck-Institute for Meteorology, Germany
MPI-ESM1-2-LR	Max-Planck-Institute for Meteorology, Germany
MRI-ESM2-0	Meteorological Research Institute, Japan
NorESM2-LM	Norwegian Climate Center, Norway
NorESM2-MM	Norwegian Climate Center, Norway
TaiESM1	Research Center for Environmental Changes, Nankang, Taipei
UKESM1-0-LL	Hadley Centre for Climate Prediction and Research, UK

The models provide simulated near-surface-temperature (tas), precipitation (pr) and soil moisture (mrso) at the Climate Model Intercomparison (CMIP6) project[24] data repository, for the period 1850-2099 and the SSP585 scenario. All available models were employed; only one simulation per model has been included to avoid biases towards models with larger simulation ensembles.

evaluation thus represents a conservative date since nearly all of the cells in the SW spatial domain pass these tests and remain in the reconstruction to that time.

The Living Blended Drought Atlas provides only EV reconstructions; we indirectly estimated CIs for its lowess values by proportionately rescaling the SPEI lowess CIs to the scale of the PMDI values (cf. Fig. 5).

Climate model simulations. The primary MODEL simulations are drawn from the sixth Climate Model Intercomparison Project (CMIP6)[24]. We screened the available models for those providing output for both for the historical period (1850-2014) and for the future under the SSP585 emissions scenario. The list of models and runs utilized is provided in Table 2. We extracted CY annual average temperature and WY cumulative precipitation for the SW region, along with MODEL soil moisture as described below. The MODEL data cover the period 1850-2099. SSP585 was selected as providing the most distinct scenario. For comparison purposes, we also examined the predecessor CMIP5[25] simulations under the similarly strongly forced RCP8.5 scenario, along with the RCP4.5 scenario as a suitable representative of less strong

anthropogenic forcing. In this case we avoided repetition of models that differ only slightly in model version, but are structurally very similar. (Table 3). For the CMIP5 outcomes the period is 1861–2095, the years of full overlap of the simulations identified.

To provide a self-consistent RECON + INST + MODEL view of the SW moisture balance from 1571 to 2099, we calibrated MODEL simulated soil moisture for each scenario to the INST SPEI values over the period 1901-2019, by mean and variance matching. We used total integrated column soil moisture, as each model constructs it. We note that directly emulating the calculation of INST SPEI observations using MODEL output would result in a metric that, in fact, reflects a soil moisture proxy (the original motivation for SPEI[20]) less well than the simulated soil moisture itself. This situation arises because the models calculate soil moisture at their native time step (e.g., 30 min), rather than employing monthly or daily averages as is done for INST SPEI observations. By construction, even daily mean data cannot capture diurnal changes, and since evaporation is non-linear a daily mean evaporation value can be very different from its incorporated evaporation trajectory, e.g., for a day with a hot afternoon and cold night, which can readily be the

Table 3 List of CMIP5 climate models used in this study.

Model	Institution
ACCESS1-0	Commonwealth Scientific and Industrial Research Organisation, Australia
ACCESS1-3	Commonwealth Scientific and Industrial Research Organisation, Australia
bcc-csm1-1	Beijing Climate Center Climate System Model, China
BNU-ESM	Beijing Normal University Earth System Model, China
CanESM2	Canadian Centre for Climate Modelling and Analysis, Canada
CCSM4	University Corporation for Atmospheric Research, USA
CESM1-BGC	University Corporation for Atmospheric Research, USA
CESM1-WACCM	University Corporation for Atmospheric Research, USA
CSIRO-Mk3-6-0	Commonwealth Scientific and Industrial Research Organisation, Australia
FGOALS-g2	State Key Laboratory of Numerical Modeling for Atmospheric Sciences and Geophysical Fluid Dynamics, China
GFDL-CM3	Geophysical Fluid Dynamics Laboratory, US
GFDL-ESM2G	Geophysical Fluid Dynamics Laboratory, US
GISS-E2-R	NASA Goddard Institute for Space Studies, US
GISS-E2-H	NASA Goddard Institute for Space Studies, US
HadGEM2-E	Hadley Centre for Climate Prediction and Research, UK
INMCM	Russian Institute for Numerical Mathematics
MIROC-ESM	University of Tokyo/NIES/JAMSTEC
MPI-ESM-LR	Max-Planck-Institute for Meteorology, Germany
MRI-CGCM3	Meteorological Research Institute, Japan
NorESM1-ME	Norwegian Climate Center, Norway

The models provide simulated near-surface-temperature (tas), precipitation (pr) and soil moisture (mrso) at the Climate Model Intercomparison (CMIP5) project[25] data repository, for at least the period 1861–2005 for the historical simulations and 2006–2095 for the scenarios simulations (RCP45 and RCP85). Only one simulation per model has been included in the study to avoid biases towards models with larger simulation ensembles.

case in much of the SW. Therefore, we determined that extracting MODEL soil moisture, a simple input-output bucket model whose physical properties vary at the scale of sub-continental regions the size of the SW[48], and then calibrating it to INST SPEI observations would be parsimonious for extension of the INST and RECON SPEI time series in comparison to emulating SPEI calculations within the model context—also bearing in mind the inherent variability and potential amplitude non-representativeness of MODEL precipitation[26]. The calibration was done for the MODEL median data and the resultant time series were then regressed on their corresponding uncalibrated data; these regressions were applied in turn to the MODEL 20% and 80% soil moisture time series to provide the 20% and 80% simulated SPEI values from 2021 onwards. The same calibration process was used with the PMDI data. We note Cook et al.[13] where these issues are discussed at length, along with Smerdon et al.[49] where bridging across RECON + INST + MODEL data is evaluated and mean and variance matching recommended.

Sea level pressure (SLP) data and reconstruction for North-eastern Pacific/Coastal Western North America Region. The SLP INST data are from the NCEP-NCAR reanalysis product[23]. The spatial SLP RECON is that of Wahl et al.[22], using an analog data-model assimilation methodology as described in the SM therein and also in Diaz et al.[50]. The climatology for both INST and RECON anomalies was set as their common period of overlap, 1948–1980, and the mean and standard deviation of the RECON data were set to match those of INST during this period to allow direct amplitude comparability between the early and current bidecadal drought periods. We note that these adjustments were quite small.

Data availability
Data availability for CMIP5[25] model output (Table 3, Fig. 5) is at http://esgf-node.llnl.gov; and for CMIP6[24] model output (Table 2, Figs. 4, 5) at https://esgf-node.llnl.gov/

search/cmip6/. Paleoreconstructions are available from the World Data Service for Paleoclimatology/NOAA National Centers for Environmental Information (WDS Paleo). SW precipitation[16,17] (Figs. 1–3, Supplementary Fig. 1) is available at https://www.ncdc.noaa.gov/paleo/study/21793. SW temperature[19] (Figs. 1–3, Supplementary Fig. 1) is available at https://www.ncdc.noaa.gov/paleo/study/12890. SW Living Blended Drought Atlas PMDI[21], reconstructed and instrumental, (Figs. 5, 6) is available at https://www.drought.gov/data-maps-tools/living-blended-drought-product-lbdp-historical-drought-information. Northeastern Pacific SLP[22] (Fig. 7) is available at https://www.ncei.noaa.gov/access/paleo-search/study/26030. Reconstructed SPEI (this article) (Fig. 5) is available upon publication at https://www.ncei.noaa.gov/access/paleo-search/study/36693. Instrumental SW precipitation and temperature[18] (Figs. 1–3) are available at https://www.ncdc.noaa.gov/cag/regional/time-series. Instrumental SPEI[20] is available at https://spei.csic.es/.

References
1. US Census Bureau. https://www2.census.gov/programs-surveys/popest/tables/2010-2019/state/totals/nst-est2019-01.xlsx (2021). Accessed 29 Sep 2021.
2. US Bureau of Economic Analysis. https://www.bea.gov/system/files/2019-04/qgdpstate0519_4.pdf (2021). Accessed 29 Sep 2021.
3. World Bank. GDP (current US$). https://data.worldbank.org/indicator/NY.GDP.MKTP.CD?most_recent_value_desc=true (2022). Accessed 21 May 2022.
4. World Shipping. https://www.worldshipping.org/top-50-ports (2021). Accessed 29 Sep 2021.
5. US Bureau of Reclamation. https://www.usbr.gov/lc/region/g4000/hourly/mead-elv.html (2022). Accessed 11 May 2022.
6. US Bureau of Reclamation. https://www.usbr.gov/rsvrWater/HistoricalApp.html;jsessionid=agetsjdGcHMRc0N3sEebDbjcUv3u7au6xTjuyhBH.lxwf01:prod_rsvrwater_ha (2022). Accessed 11 May 2022.
7. Schwartz, A. I'm a Scientist in California. Here's What Worries Me Most About Drought. *New York Times.* https://www.nytimes.com/2022/04/04/opinion/environment/california-drought-wildfires.html (2022). Accessed 11 May 2022.
8. Purtill, C. A drought so bad it exposed a long-ago homicide. Getting the water back will be harder than ever. *Los Angeles Times.* https://www.latimes.com/environment/story/2022-05-06/climate-change-makes-it-harder-to-

get-water-needed-to-end-california-megadrought (2022). Accessed 11 May 2022.

9. Cook, E. R. et al. Megadroughts in North America: placing IPCC projections of hydroclimatic change in a long-term palaeoclimate context. *J. Quat. Sci.* **25**, 48–61 (2010).

10. Woodhouse, C. A., Meko, D. M., MacDonald, G. M. & Stahle, D. W. A 1,200-year perspective of 21st century drought in southwestern North America. *Proc. Natl Acad. Sci. USA* **107**, 21283–21288 (2010).

11. Cook, B. I., Ault, T. R. & Smerdon, J. E. Unprecedented 21st century drought risk in the American Southwest and Central Plains Drought risk in Western North America. *Sci. Adv.* **1**, e00082 (2015).

12. Ault, T. R., Mankin, J. S., Cook, B. I. & Smerdon, J. E. Relative impacts of mitigation, temperature, and precipitation on 21st-century megadrought risk in the American Southwest. *Sci. Adv.* **2**, e1600873 (2016).

13. Cook, B. I. et al. North American megadroughts in the Common Era: reconstructions and simulations. *WIREs Clim. Change* **7**, 411–432 (2016).

14. Williams, A. P. et al. Large contribution from anthropogenic warming to an emerging North American megadrought. *Science* **368**, 314–318 (2020).

15. Williams, A. P., Cook, B. I. & Smerdon, J. E. Rapid intensification of the emerging southwestern North American megadrought in 2020–2021. *Nat. Clim. Change* **12**, 232–234 (2022).

16. Diaz, H. F. & Wahl, E. Recent California Water Year Precipitation Deficits: A 440-year Perspective. *J. Clim.* **28**, 4637–4652 (2015).

17. Wahl, E., Diaz, H. F., Vose, R. & Gross, W. Multicentury evaluation of recovery from strong precipitation deficits in California. *J. Clim.* **30**, 6053–6063 (2017).

18. NOAA Climate at a Glance, National Centers for Environmental Information. https://www.ncdc.noaa.gov/cag/regional/time-series (2021). Accessed 29 June and 24 October, 2021.

19. Wahl, E. & Smerdon, J. Comparative performance of paleoclimate field and index reconstructions derived from climate proxies and noise-only predictors. *Geophys. Res. Lett.* **39**, L06703 (2012).

20. Consejo Superior de Investigaciones Científicas de España (CSIC). https://spei.csic.es/ (2021). Accessed 29 Sep 2021.

21. NOAA. https://www.drought.gov/data-maps-tools/living-blended-drought-product-lbdp-historical-drought-information (2021). Accessed 29 Sep 2021.

22. Wahl, E., Hoell, A., Zorita, E., Gille, E. & Diaz, H. F. A 450-year perspective on california precipitation "flips". *J. Clim.* **33**, 10221–10237 (2020).

23. Kalnay, E. et al. The NCEP/NCAR 40-year reanalysis project. *Bull. Am. Meteorol. Soc.* **77**, 437–471 (1996).

24. O'Neill, B. C. et al. The Scenario Model Intercomparison Project (ScenarioMIP) for CMIP6. *Geosci. Model Dev.* **9**, 3461–3482 (2016).

25. Taylor, K. E., Stouffer, R. J. & Meehl, G. A. An overview of CMIP5 and the experiment design. *Bull. Am. Meteorol. Soc.* **93**, 485–498 (2012).

26. Schmidt, D. F. & Grise, K. M. Drivers of Twenty-First-Century US Winter Precipitation Trends in CMIP6 Models: a storyline-based approach. *J. Clim.* **34**, 6875–6889 (2021).

27. IPCC, 2021: Summary for Policymakers. In: *Climate Change 2021: The Physical Science Basis. Contribution of Working Group I to the Sixth Assessment Report of the Intergovernmental Panel on Climate Change* (et al. MassonDelmotte, V. P. et al.) (Cambridge University Press, 2021).

28. Wahl, E., Diaz, H. F., Smerdon, J. & Ammann, C. Late Winter Temperature Response to Large Tropical Volcanic Eruptions in Temperate Western North America: Relationship to ENSO Phases. *Glob. Planet. Change.* **122**, 238–250 (2014).

29. Cook, B. I., Smerdon, J. E., Seager, R. & Coats, S. Global warming and 21st century drying. *Climate Dynamics* **43**, 2607–2627 (2014).

30. Wells, N., Goddard, S. & Hayes, M. J. A Self-Calibrating Palmer Drought Severity Index. *J. Clim.* **17**, 2335–2351 (2004).

31. Gangopadhyay, S., Woodhouse, C. A., McCabe, G. J., Routson, C. C. & Meko, D. M. Tree rings reveal unmatched 2nd century drought in the Colorado River Basin. *Geophys. Res. Lett.* **49**, e2022GL098781 (2022).

32. Cook, B. et al. Uncertainties, limits, and benefits of climate change mitigation for soil moisture drought in Southwestern North America. Abstract GC22B-02, American Geophysical Union Fall Conference 2021, 13-17 December, 2021, New Orleans, Louisiana, USA. https://agu.confex.com/agu/fm21/meetingapp.cgi/Paper/792499 (2021). Accessed 17 Dec 2021.

33. Swann, A. L., Hoffman, F. M., Koven, C. D. & Randerson, J. T. Plant responses to increasing CO_2 reduce estimates of climate impacts on drought severity. *Proc. Natl. Acad. Sci. USA* **113:36**, 10019–10024 (2016).

34. Mankin, J. S., Smerdon, J. E., Cook, B. I., Williams, A. P. & Seager, R. The curious case of projected twenty-first-century drying but greening in the American West. *J. Clim* **30:21**, 8689–8710 (2017).

35. Wahl, E., Zorita, E., Trouet, V. & Taylor, A. Jet stream dynamics, hydroclimate, and fire in California: 1600-2000 CE. *Proc. Natl. Acad. Sci. USA* **116:12**, 5393–5398 (2019).

36. López, J., Way, D. A. & Sadok, W. Systemic effects of rising atmospheric vapor pressure deficit on plant physiology and productivity. *Glob. Chang. Biol.* **27**, 1704–1720 (2021).

37. Yuan, W. et al. Increased atmospheric vapor pressure deficit reduces global vegetation growth. *Sci. Adv.* **5**, eaax1396 (2019).

38. St. George, S., Meko, D. & Cook, E. The seasonality of precipitation signals embedded within the North American Drought Atlas. *Holocene* **20**, 983–988 (2010).

39. NOAA. Drought Task Force Report 2020-2021 Southwestern US Drought, https://www.drought.gov/documents/noaa-drought-task-force-report-2020-2021-southwestern-us-drought. (2021). Accessed 19 Oct 2021.

40. North, G. R., Cahalan, R. F. & Coakley, J. A. Jr Energy balance climate models. *Rev. Geophys.* **19**, 91–121 (1982).

41. Ashfaq, M. et al. Near-term acceleration of hydroclimatic change in the western US. *J. Geophys. Res. Atmos.* **118**, 10676–10693 (2013).

42. Wi, S. et al. Climate change projections of snowfall in the Colorado River Basin using dynamical downscaling. *Water Resour. Res.* **48**, W05504 (2012).

43. Abatzoglou, J. T. & Williams, A. P. Impact of anthropogenic climate change on wildfire across western US forests. *Proc. Natl. Acad. Sci. USA* **113**, 11770–11775 (2016).

44. Huang, X., Hall, A. D. & Berg, N. Anthropogenic warming impacts on today's Sierra Nevada snowpack and flood risk. *Geophys. Res. Lett.* **45**, 6215–6222 (2018).

45. Rodziewicz, D., Amante, C. J., Dice, J. & Wahl, E. Housing market impairment from future sea-level rise inundation. *Environment Systems And Decisions* (published online 08 Feb 2022), https://doi.org/10.1007/s10669-022-09842-6 (2022).

46. PAGES 2k Consortium Continental-scale temperature variability during the last two millennia. *Nat. Geosci.* **6**, 339–346, https://doi.org/10.1038/NGEO1797 (2013).

47. Trouet, V. et al. A 1500-year reconstruction of annual mean temperature for temperate North America on decadal-to-multidecadal time scales. *Environ. Res. Lett.* **8**, 024008 (2013).

48. Garfin, G. et al. *United States Fourth National Climate Assessment* (eds. Reidmiller et al.) Ch. 25, 1101–1184 (U.S. Global Change Research Program, 2018). https://doi.org/10.7930/NCA4.2018.CH25.

49. Smerdon, J. E., Cook, B. I., Cook, E. R. & Seager, R. Bridging past and future climate across paleoclimatic reconstructions, observations, and models: a hydroclimate case study. *J. Clim.* **28**, 3212–3231 (2015).

50. Diaz, H. F., Wahl, E., Zorita, E., Giambelluca, T. & Eischeid, J. A 480-year reconstruction of Hawaiian islands rainfall. *J. Clim.* **29**, 5661–5674 (2016).

Acknowledgements

Author contributions

E.R.W. conceived and designed the study, performed analyses, and wrote the paper. E.Z. assisted in designing the study, performed analyses, and assisted in writing the paper. H.F.D. assisted in designing the study, interpreting results, and writing the paper. A.H. assisted in designing the study, interpreting results, and writing the paper.

Competing interests

The authors declare no competing interests.

Additional information